ARMY RESEARCH LABORATORY

Plasticity and Spall in High Density Polycrystals: Modeling and Simulation

by John D. Clayton

ARL-RP-153 **September 2006**

A reprint from *the APS SCCM Conference Proceedings*,
American Institute of Physics, pp. 311–314, 2006.

NOTICES

Disclaimers

The findings in this report are not to be construed as an official Department of the Army position unless so designated by other authorized documents.

Citation of manufacturer's or trade names does not constitute an official endorsement or approval of the use thereof.

Destroy this report when it is no longer needed. Do not return it to the originator.

Army Research Laboratory
Aberdeen Proving Ground, MD 21005-5066

ARL-RP-153 **September 2006**

Plasticity and Spall in High Density Polycrystals: Modeling and Simulation

John D. Clayton
Weapons and Materials Research Directorate, ARL

A reprint from *the APS SCCM Conference Proceedings*,
American Institute of Physics, pp. 311–314, 2006.

REPORT DOCUMENTATION PAGE

Form Approved
OMB No. 0704-0188

1. REPORT DATE *(DD-MM-YYYY)*	2. REPORT TYPE	3. DATES COVERED (From - To)
September 2006	Reprint	2003–2006

4. TITLE AND SUBTITLE
Plasticity and Spall in High Density Polycrystals: Modeling and Simulation

5a. CONTRACT NUMBER

5b. GRANT NUMBER

5c. PROGRAM ELEMENT NUMBER

6. AUTHOR(S)
John D. Clayton

5d. PROJECT NUMBER
WHPR01B

5e. TASK NUMBER

5f. WORK UNIT NUMBER

7. PERFORMING ORGANIZATION NAME(S) AND ADDRESS(ES)
U.S. Army Research Laboratory
ATTN: AMSRD-ARL-WM-TD
Aberdeen Proving Ground, MD 21005-5066

8. PERFORMING ORGANIZATION REPORT NUMBER
ARL-RP-153

9. SPONSORING/MONITORING AGENCY NAME(S) AND ADDRESS(ES)

10. SPONSOR/MONITOR'S ACRONYM(S)

11. SPONSOR/MONITOR'S REPORT NUMBER(S)

12. DISTRIBUTION/AVAILABILITY STATEMENT
Approved for public release; distribution is unlimited.

13. SUPPLEMENTARY NOTES
A reprint from the *APS SCCM Conference Proceedings*, American Institute of Physics, pp. 311–314, 2006.

14. ABSTRACT
The high strain rate behavior of multiphase, high density metallic polycrystals is studied via constitutive modeling and numerical simulation. Crystalline elasto-plasticity models are developed to account for the thermomechanical response of each bulk phase, and a cohesive zone approach is invoked to model the response of grain and phase boundaries. The following physical phenomena are captured by the bulk constitutive models: finite deformations, temperature- and pressure-dependent elasticity, nonlinear thermal expansion, slip-system level viscoplasticity with thermal softening due to increasing dislocation mobility, and dislocation accumulation in conjunction with strain hardening and the stored energy of cold working. The cohesive laws account for stress-state and temperature effects on interfacial strengths and correlate with the spall strength of the multiphase material. Numerical results are obtained from a 2D finite element implementation of the model under impact loading, in which individual phases, grains, and interfaces within a two-phase tungsten alloy are fully resolved. Effects of lattice orientations, grain morphology, and cohesive model parameters are reflected in the spall behavior and statistics associated with predicted free surface velocity profiles.

15. SUBJECT TERMS
microstructure modeling, plasticity, spall fracture, tungsten

16. SECURITY CLASSIFICATION OF:			17. LIMITATION OF ABSTRACT	18. NUMBER OF PAGES	19a. NAME OF RESPONSIBLE PERSON
a. REPORT	b. ABSTRACT	c. THIS PAGE			John D. Clayton
UNCLASSIFIED	UNCLASSIFIED	UNCLASSIFIED	UL	10	19b. TELEPHONE NUMBER (*Include area code*) 410-306-0975

CP845, *Shock Compression of Condensed Matter - 2005,*
edited by M. D. Furnish, M. Elert, T. P. Russell, and C. T. White

PLASTICITY AND SPALL IN HIGH DENSITY POLYCRYSTALS: MODELING AND SIMULATION

John D. Clayton[1]

[1]*Impact Physics Branch, U.S. Army Research Laboratory, Aberdeen Proving Ground, MD 21005-5069*

Abstract. The high strain rate behavior of multiphase, high density metallic polycrystals is studied via constitutive modeling and numerical simulation. Crystalline elasto-plasticity models are developed to account for the thermomechanical response of each bulk phase, and a cohesive zone approach is invoked to model the response of grain and phase boundaries. The following physical phenomena are captured by the bulk constitutive models: finite deformations, temperature- and pressure-dependent elasticity, nonlinear thermal expansion, slip-system level viscoplasticity with thermal softening due to increasing dislocation mobility, and dislocation accumulation in conjunction with strain hardening and the stored energy of cold working. The cohesive laws account for stress-state and temperature effects on interfacial strengths and correlate with the spall strength of the multiphase material. Numerical results are obtained from a 2D finite element implementation of the model under impact loading, in which individual phases, grains, and interfaces within a two-phase tungsten alloy are fully resolved. Effects of lattice orientations, grain morphology, and cohesive model parameters are reflected in the spall behavior and statistics associated with predicted free surface velocity profiles.

Keywords: tungsten, microstructure modeling, plasticity, spall fracture.
PACS: 02.70.Dh, 62.20.-x, 62.50.+p, 83.60.-a.

INTRODUCTION

This work investigates the dynamic response of a two-phase tungsten alloy of interest to the defense industry for use in Kinetic Energy (KE) penetration applications [1]. The material consists of pure tungsten (W) grains of body-centered-cubic structure embedded in a face-centered-cubic binder phase of W, nickel (Ni), and iron (Fe). In what follows, we develop crystal plasticity-based constitutive models for each phase that account for the effects of initial lattice orientation (i.e., texture) on the anisotropic stress-strain response [2, 3]. Additionally, cohesive zone models are formulated that account for separation at grain and phase boundaries as a result of the resolved stress components acting on these boundaries, and reflecting the experimentally observed increase in fracture toughness with increasing temperature, i.e., a brittle-to-ductile transition [4]. The theory is implemented in a dynamic Lagrangian finite element (FE) code [5], and 2D FE meshes are constructed of the initial microstructures of a KE rod sectioned either transversely or parallel to the rod axis (i.e., the extrusion direction). Simulations of high rate impact, wave propagation, and spall are conducted, reminiscent of conditions present in plate impact experiments [6, 7]. We show how statistical data acquired from simulations depict effects of the microstructure and model parameters.

THEORY

Only essential aspects of the constitutive theory are given here; the interested reader may

find more details in the references [2,3]. The kinematics of thermo-elastoplasticity within each phase of the bulk material is described by the following decomposition of the deformation gradient **f**:

$$\mathbf{f} = \partial \mathbf{x} / \partial \mathbf{X} = \mathbf{f}^{\mathbf{e}} \mathbf{f}^{\boldsymbol{\theta}} \mathbf{f}^{\mathbf{p}}, \tag{1}$$

where $\mathbf{f}^{\mathbf{e}}$ accounts for rotation of the lattice and stretching due to applied stresses, $\mathbf{f}^{\boldsymbol{\theta}}$ reflects stress-free isotropic thermal expansion/contraction, and $\mathbf{f}^{\mathbf{p}}$ is the plastic stretch and rotation due to inelastic mechanisms, namely dislocation glide. Spatial and referential coordinates are denoted by **x** and **X**, respectively. The free energy per unit mass ψ of each crystal is decomposed as

$$\begin{aligned} \rho\psi = {} & \frac{1}{2} K_0(\theta)\vartheta^2 - \frac{1}{3} K_1 \vartheta^3 + \\ & \mu(\theta)\mathbf{e}^{\mathbf{e}\prime} : \mathbf{e}^{\mathbf{e}\prime} + \frac{1}{2}\kappa\mu(\theta)\xi^2 + y(\theta), \end{aligned} \tag{2}$$

where ρ is the mass density in the intermediate configuration, θ is the temperature, ϑ and $\mathbf{e}^{\mathbf{e}\prime}$ are respectively the scalar elastic volumetric strain and the elastic deviatoric strain tensor in the intermediate frame, ξ is an internal variable associated with the internal energy contribution from the microscopic stress fields of lattice defects, and y accounts for the specific heat. The nominal bulk modulus and shear modulus are given by K_0 and μ, respectively, κ is a scalar parameter, and a K_1 leads to a volume- (i.e. pressure-) dependent effective bulk modulus. Note that W is virtually elastically isotropic at room temperature and low pressure. The local energy balance is written as

$$\begin{aligned} \underbrace{\rho\hat{c}\dot{\theta}}_{\text{temperature change}} = {} & \underbrace{\sum_{\alpha=1}^{n} \tau^{(\alpha)}\dot{\gamma}^{(\alpha)}}_{\text{plastic dissipation}} - \underbrace{\rho\left(\left(\partial_{\xi}\psi\right) - \theta\left(\partial_{\theta\xi}\psi\right)\right)\dot{\xi}}_{\text{energy of lattice defects}} \\ & + \underbrace{\rho\theta\partial_{\theta\mathbf{e}}\psi : \dot{\mathbf{e}}}_{\text{thermoelastic coupling}} + \underbrace{div\left(k\nabla_{\mathbf{x}}\theta\right)}_{\text{heat conduction}}, \end{aligned} \tag{3}$$

where ρ is the spatial mass density, $\hat{c}$ is the specific heat capacity, $\tau^{(\alpha)}$ is the resolved Cauchy stress on slip system α, $\dot{\gamma}^{(\alpha)}$ is the plastic slip rate, and k is the thermal conductivity. The viscoplastic flow rule is given by

$$\dot{\gamma}^{(\alpha)} = \dot{\gamma}_0 \left(\frac{\tau^{(\alpha)}}{g^{(\alpha)}} \right)^m \operatorname{sgn}\left(\tau^{(\alpha)}\right), \tag{4}$$

with $\tau^{(\alpha)}$ the resolved Kirchhoff stress, $g^{(\alpha)}$ the evolving temperature-dependent slip resistance, and $\dot{\gamma}_0$ and m material parameters.

Interface separation is modeled by the cohesive zone approach, whereby crack initiation occurs when the resolved local stress component(s) exceed a user-prescribed value. In the present work, fractures occur when one of the following criteria is achieved locally:

$$\hat{s} = \hat{s}_0 + \hat{s}_1(\theta - \theta_0), \qquad \hat{\tau} = \hat{\tau}_0 + \hat{\tau}_1(\theta - \theta_0), \tag{5}$$

where $\hat{s}$ is the resolved nominal normal stress at the interface, $\hat{\tau}$ is the resolved nominal shear stress at the interface, and the remaining symbols entering Eq. (5) are material parameters. Upon damage initiation, the response of the degraded material at interfaces is dictated by the following irreversible traction-displacement relations:

$$\begin{aligned} \hat{s} &= \left(\hat{s}_0 + \hat{s}_1(\theta - \theta_0)\right)\left(1 - \frac{\delta_n}{\delta_c}\right), && \text{(load)} \\ \hat{s} &= \left(\hat{s}_0 + \hat{s}_1(\theta - \theta_0)\right)\left(1 - \frac{\delta_{n1}}{\delta_c}\right)\frac{\delta_n}{\delta_{n1}}, && \text{(unload)} \end{aligned} \tag{6}$$

$$\begin{aligned} \hat{\tau} = {} & \left(\hat{\tau}_0 + \hat{\tau}_1(\theta - \theta_0)\right)\times \\ & \left(1 - \frac{|\delta_t|}{\delta_c}\right)\left(1 - \frac{\langle \delta_n \rangle}{\delta_c}\right)\operatorname{sgn}(\delta_t), \quad \text{(load)} \\ \hat{\tau} = {} & \left(\hat{\tau}_0 + \hat{\tau}_1(\theta - \theta_0)\right)\times \\ & \left(1 - \frac{|\delta_{t1}|}{\delta_c}\right)\left(1 - \frac{\langle \delta_n \rangle}{\delta_c}\right)\frac{\delta_t}{|\delta_{t1}|}, \quad \text{(unload)} \end{aligned} \tag{7}$$

with δ_n the normal crack opening displacement, δ_{n1} the maximum previous value of δ_n, δ_t the tangential opening displacement, δ_{t1} the maximum previous value of δ_t, and δ_c a material parameter defining the separation distance beyond which the damaged zone behaves as two free surfaces.

NUMERICAL IMPLEMENTATION

The constitutive models for the pure W and binder phases, as well as those for cohesive interfaces, were implemented within the EPIC dynamic finite element program [5]. For details regarding the FE implementation, please see [3].

Unstructured finite element meshes conforming to realistic microstructures were constructed from optical images of tungsten alloy KE rods, as depicted in Fig. 1 and Fig. 2. Initial lattice orientations of the grains were designated to match experimentally-obtained data from an electron backscattering diffraction technique. The domain size was $L = 150\ \mu$m, and on the order of 20000 plane strain triangular elements were used, with more refined areas of the mesh concentrated in the vicinity of grain and phase boundaries. The OOF meshing software [8] was used to this end. Four-node cohesive elements were inserted along these boundaries, with coincident nodes constrained to remain rigidly bonded in the simulations until either of the criteria (5) was attained.

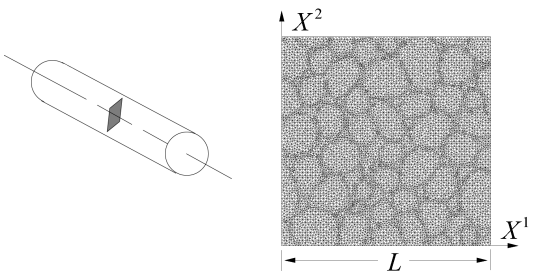

Figure 1. Transverse section of KE rod and FE mesh of corresponding equiaxed granular microstructure.

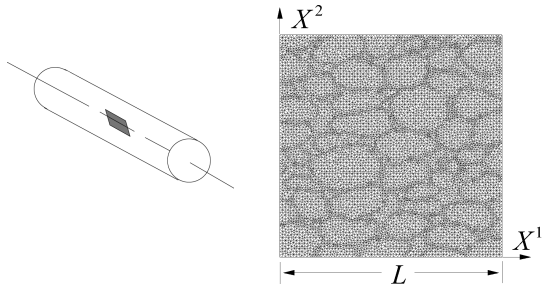

Figure 2. Longitudinal section of KE rod and FE mesh of corresponding elongated granular microstructure.

RESULTS AND DISCUSSION

Here we report on impact, wave propagation, and spall behavior of the tungsten alloy. For these simulations, the following boundary conditions were applied:

- Along $X^1 = 0$, a short velocity impulse of duration 10 ns was applied in the positive 1-direction, corresponding to an impact velocity in a plate impact experiment of 250 m/s. Subsequently, the boundary $X^1 = 0$ was held rigid.
- Along $X^1 = L$, null traction conditions were specified.
- Along $X^2 = 0$ and $X^2 = L$, either non-reflecting conditions [5] or uniaxial strain conditions (i.e. null velocity in the 2-direction) were imposed in various simulations.
- Null heat flux conditions were specified along all external surfaces.

The above boundary conditions create a rightward-moving compressive wave that travels through the grid, reflects off the free surface at $X^1 = L$ as a tensile wave, then potentially leading to spall fracture within the sample.

Deformed FE meshes for an equiaxed microstructure in Fig. 3, at an elapsed simulation time of 100 ns, illustrate the spall separation at the material interfaces. On the left image in Fig. 3, we used $\hat{s}_1 = \hat{\tau}_1 = 0$ in Eqs. (5)-(7), meaning that the brittle-ductile transition was not addressed. On the

right image of Fig. 3, nonzero values were used for $\hat{s}_1$ and $\hat{\tau}_1$. Different fracture patterns emerge, with fracture suppressed in the right figure relative to the left due to cohesive strengthening following the temperature rise that occurs commensurate with wave propagation and plastic dissipation.

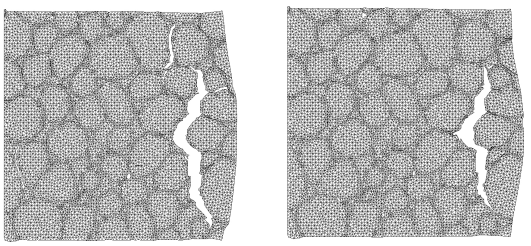

FIGURE 3. Deformed FE meshes at t = 100 ns. Temperature-independent cohesive law used on left simulation, temperature-dependent law used on right.

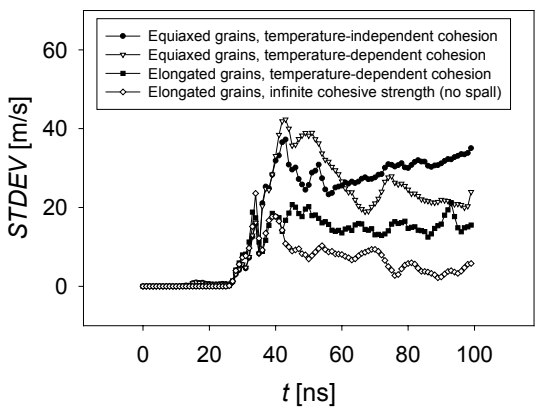

Figure 4. Standard deviation in free surface velocity for selected simulations featuring various microstructures and cohesive parameters.

Figure 4 shows the time history of the standard deviation in the free surface velocities recorded at $X^1 = L$. Prior to $t \approx 25$ ns, velocities are zero as the compressive wave has not yet reached the surface. We see that the velocity statistics are influenced by grain shape (i.e., equiaxed versus elongated) and choice of cohesive parameters. In the extreme case of infinite cohesive strength in which spall fractures are suppressed, the standard deviation values are generally much smaller than the other cases in which spallation occurs.

CONCLUSIONS

A numerical model of plastic deformation and spallation in multiphase metallic crystals has been exercised, capturing finite anisotropic elasto-plasticity, thermodynamics of energy storage, dissipation, and heat conduction, as well as interfacial fracture. The results presented here indicate relationships between microstructural features, fracture patterns, and free surface velocity statistics. Such information should provide increased understanding of experimentally-obtained results from plate impact tests [6, 7].

ACKNOWLEDGEMENTS

Support from the Weapons and Materials Research Directorate of the U.S. Army Research Laboratory is acknowledged.

REFERENCES

1. Magness, L.S., "High strain rate deformation behaviors of kinetic energy penetrator materials during ballistic impact", Mech. Mater. 17, 147-154, 1994.
2. Clayton, J.D., "Dynamic plasticity and fracture in high density polycrystals: constitutive modeling and numerical simulation", J. Mech. Phys. Solids 53, 261-301, 2005.
3. Clayton, J.D., "Modeling dynamic plasticity and spall fracture in high density polycrystalline alloys", Int. J. Solids Structures 42, 4613-4640, 2005.
4. O'Donnell, R.G. and Woodward, R.L., "Influence of temperature on the fracture of a W-Ni-Fe alloy", J. Mater. Sci. 35, 4319-4324, 2000.
5. Johnson, G.R., Stryk, R.A., Holmquist, T.J., and Beissel, S.R., "Numerical algorithms in a Lagrangian hydrocode" , Wright Laboratory, U.S.A., WL-TR-1997-7039, 1997.
6. Vogler, T.J., Reinhart, W.D., and Chhabildas, L.C., "Dynamic behavior of boron carbide", J. Appl. Phys. 95, 4173-4183, 2004.
7. Vogler, T.J. and Clayton, J.D., "Heterogeneous spall failure of a tungsten alloy", Proc. Soc. for Experimental Mechanics Annual Conference and Exposition, Portland, OR, USA, June 7-9, 2005.
8. Langer, S., Reid, A., Carter, C., Fuller, E., and Roosen, A., *PPM2OOF v1.1*, freeware website http://www.ctcms.nist.gov/, 2003.

NO. OF COPIES	ORGANIZATION
1 (PDF ONLY)	DEFENSE TECHNICAL INFORMATION CTR DTIC OCA 8725 JOHN J KINGMAN RD STE 0944 FORT BELVOIR VA 22060-6218
1	US ARMY RSRCH DEV & ENGRG CMD SYSTEMS OF SYSTEMS INTEGRATION AMSRD SS T 6000 6TH ST STE 100 FORT BELVOIR VA 22060-5608
1	DIRECTOR US ARMY RESEARCH LAB IMNE ALC IMS 2800 POWDER MILL RD ADELPHI MD 20783-1197
3	DIRECTOR US ARMY RESEARCH LAB AMSRD ARL CI OK TL 2800 POWDER MILL RD ADELPHI MD 20783-1197

ABERDEEN PROVING GROUND

1	DIR USARL AMSRD ARL CI OK TP (BLDG 4600)

NO. OF
COPIES ORGANIZATION

ABERDEEN PROVING GROUND

32 DIR USARL
AMSRD ARL CI HC
P CHUNG
AMSRD ARL WM
J MCCAULEY
T WRIGHT
AMSRD ARL WM MA
W NOTHWANG
AMSRD ARL WM TA
S SCHOENFELD
AMSRD ARL WM TC
M FERMEN COKER
R COATES
AMSRD ARL WM TD
S BILYK
T BJERKE
D CASEM
J CLAYTON (5 CPS)
T CLINE
D DANDEKAR
W EDMANSON
M GREENFIELD
C GUNNARSSON
Y HUANG
K IYER
R KRAFT
B LOVE
S MCNEILL
H MEYER
R MUDD
M RAFTENBERG
E RAPACKI
M SCHEIDLER
S SEGLETES
T WEERASOORIYA